THE JOURNAL OF PHYSICAL CHEMISTRY A
A JOURNAL OF THE AMERICAN CHEMICAL SOCIETY

pubs.acs.org/JPCA

Article

Ultrafast Evaluation of Two-Photon Absorption with Simplified Time-Dependent Density Functional Theory

Marc de Wergifosse,* Pierre Beaujean, and Stefan Grimme

Cite This: *J. Phys. Chem. A* 2022, 126, 7534−7547

Read Online

ACCESS | Metrics & More | Article Recommendations | Supporting Information

ABSTRACT: This work presents the theoretical background to evaluate two-photon absorption (2PA) cross-sections in the framework of simplified time-dependent density functional theory (sTD-DFT). Our new implementation allows the ultrafast evaluation of 2PA cross-sections for large molecules based on a regular DFT ground-state determinant as well as a variant employing our tight-binding sTD-DFT-xTX flavor for very large systems. The method is benchmarked against higher-level calculations for *trans*-stilbene and typical fluorescent protein chromophores. For eGFP, a quadrupolar chromophore and its branched version, the flavine mono-nucleotide, and the iLOV protein, we compare sTD-DFT 2PA spectra to experimental ones. This includes extension and testing of our all-atom quantum chemistry methodology for the evaluation of 2PA for a system of ∼2000 atoms, providing striking agreement with the experimental spectrum.

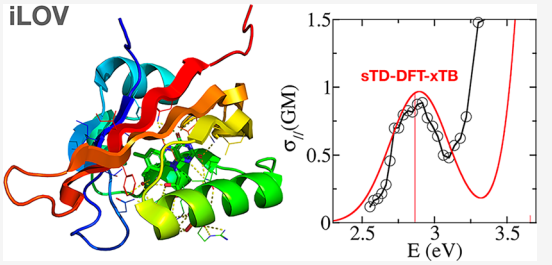

INTRODUCTION

Two-photon absorption (2PA) is a nonlinear optical phenomenon in which a compound absorbs two photons simultaneously. 2PA was first predicted theoretically in 1931 by Göppert-Mayer.[1] It is used in 2P-excited near-infrared (NIR)-emitting dyes or materials with applications in various fields such as bioimaging,[2−6] optical data storage,[7−10] microfabrication,[11,12] and photodynamic therapy.[13−17] Thus, the design of new 2P-excited NIR-emitting dyes or materials is an attractive prospect for which theoretical chemistry could play an important role.

From a theoretical point of view, computing a higher-order molecular response property such as 2PA cross-sections (σ^{2PA}) is inherently difficult.[18] In the realm of wave function methods, probably the most accurate scheme was developed by Nanda and Krylov[19] at the equation-of-motion coupled-cluster (CC) wave functions with single and double substitutions (EOM-CCSD) level of theory, but it is only applicable to relatively small systems.[20−25] Other CC methods to evaluate 2PA were implemented by Hättig et al.[26] at the CCSD, CCS, and CC2 levels of theory. A CC3 implementation also exists.[27] To provide a treatment for small-to-medium-sized molecules, Friese et al.[28] implemented the 2PA evaluation using the resolution-of-identity second-order approximate CC (RI-CC2) method, leading to a large number of applications, and used it as a reference level.[29−36] Regarding density functional theory (DFT) methods, the evaluation of σ^{2PA} with the time-dependent DFT (TD-DFT) was implemented by Salek et al.[37] in 2003. Since then, other implementations have also been reported by Zahariev and Gordon[38] and Furche and co-workers.[39] These implementations were applied to many medium-sized systems.[33,40−52] Several benchmark studies pointed out large errors for σ^{2PA} determined by TD-DFT with respect to reference RI-CC2 calculations, but range-separated hybrid exchange−correlation (XC) functionals appeared to yield more systematic results.[32−35,53] Semi-empirical methods to evaluate 2PA are also available.[54]

A particular interest in the simulation of the 2PA of fluorescent proteins (FPs) has appeared over the years,[29−32,35,55−61] but they resorted to truncated protein calculations including or not polarizable embedding (PE).[30,55,62,63] In 2014, Salem and Brown[56] assessed the performance of TD-DFT for computing 2PA cross-sections of FP chromophores with respect to CC2. They concluded that B3LYP and PBE0 functionals are well suited to screen a set of FP chromophores for 2PA. Furthermore, they reported that long-range corrected hybrid functionals performed badly for high-energy transitions of FPs. In a second study,[57] they screened FP chromophores, incorporating noncanonical amino acids in green FP (GFP) with TD-DFT. This study was reiterated but by incorporating noncanonical amino acids in the red FP.[58] In 2018, Simsek and Brown[59] combined molecular dynamics with TD-DFT calculations to investigate 2PA of the gold FP modulated by conformational changes. Note that in their 2PA calculations, only the chromophore without any protein residues was considered. In 2019,

Received: April 8, 2022
Revised: September 16, 2022
Published: October 6, 2022

https://doi.org/10.1021/acs.jpca.2c02395
J. Phys. Chem. A 2022, 126, 7534−7547

Rossano-Tapia and Brown[60] used the sum-over-states expression to evaluate 2PA cross-sections at the semiempirical time-dependent density functional tight binding (TD-DFTB2) level of theory on FP chromophores, showing that this method does not perform well.

All-atom quantum chemistry calculations of 2PA on an entire protein have never been attempted before to the best of our knowledge. This is easily explainable because the evaluation of σ^{2PA} is computer resource demanding, which cannot be applied even at a TD-DFT level to systems with a few thousands of atoms. Recently, we proposed an all-atom quantum chemistry methodology to study the second-harmonic generation of FPs based on our simplified TD-DFT (sTD-DFT) implementation.[64] We were able to reproduce the low-energy part of the experimental hyper-Rayleigh scattering first hyperpolarizability frequency dispersion of bacteriorhodopsin and further provided results for the smaller iLOV protein.

In this context, we implemented the evaluation of the 2PA cross-sections at the sTD-DFT level of theory. The computationally efficient sTD-DFT method was proposed by Grimme and co-workers[65,66] to extend the reach of TD-DFT to large systems. Considering its Tamm−Dancoff variant (sTDA),[65] Grimme globally parameterized the two integral parameters of the method for hybrid XC functionals to reproduce two standard benchmark sets considering vertical singlet−singlet excitations, providing deviations from reference data similar to those observed when using TD-DFT. Larger deviations were observed for n → π^* and metal-centered d → d excitations. It was also shown that the sTD-DFT method yields reliable oscillator and rotatory strengths.[66] The sTD-DFT method was then extended to ultralarge systems with its extended tight-binding (xTB) version.[67] Following this, we implemented a large number of methods to evaluate molecular response properties.[68−70] Taking the single residue of the sTD-DFT quadratic response,[68] a first unpublished version of the 2PA implementation was already available in 2018 as mentioned in our recent perspective article,[71] but because of an inconsistent normalization in the eigenvectors, the results were partially incorrect. The current implementation described here now fully solves this problem.

To assess the performance of the sTD-DFT 2PA implementation, we selected compounds for which reference σ^{2PA} values are available: first, *trans*-stilbene that was studied by one of us at the EOM-CCSD level of theory,[20,21] and second, FP chromophores, that is, 4-(*p*-hydroxybenzylidene)-imidazolidin-5-one (HBI), 4-(*p*-hydroxybenzylidene)-1,2-dimethylimidazolin-5-one (HBDI), the chromophore of the cyan FP (CFP), and *p*-coumaric acid (PYP, the chromophore of the phosphorescent yellow protein) for which EOM-CCSD and RI-CC2 reference σ^{2PA} values exist.[19,32,56] Then, we consider systems for which experimental 2PA spectra are available: the enhanced GFP (eGFP),[4] a quadrupolar chromophore (**A**) and its branched version (**B**),[72] the flavin mononucleotide (FMN),[30,73] and iLOV FP[73] for which the FMN is the encapsulated chromophore. This set of compounds thus includes two FPs to showcase the performance of our implementation. This extends our all-atom quantum chemistry methodology[64] to the evaluation of 2PA for iLOV.

This article is organized as follows. First, we present the theoretical background of the sTD-DFT 2PA implementation. Then, the computational details are given, and results are discussed before providing conclusions.

METHODS

Theory. Using the density-matrix-based TD-DFT formalism,[38,39,74−78] we derived the quadratic-response function in the sTD-DFT framework.[68] From it, by taking its double residue, we already showed how to evaluate state-to-state transition dipole moments.[69] The 2PA cross-sections can be obtained in the same way but from the single residue of the quadratic response function for two degenerated photon frequencies.[79] In the following, *p*, *q*, *r*, and *s* indices refer to general molecular orbitals, *i*, *j*, *k*, and *l* to occupied molecular orbitals, and *a*, *b*, *c*, and *d* to unoccupied molecular orbitals. The linear-response TD-DFT equation reads

$$\left[\begin{pmatrix}\mathbf{A} & \mathbf{B}\\ \mathbf{B} & \mathbf{A}\end{pmatrix} - \omega\begin{pmatrix}1 & 0\\ 0 & -1\end{pmatrix}\right]\begin{pmatrix}\mathbf{X}_\zeta(\omega)\\ \mathbf{Y}_\zeta(\omega)\end{pmatrix} = -\begin{pmatrix}\mu_\zeta\\ \mu_\zeta\end{pmatrix} \tag{1}$$

where $X_\zeta(\omega)$ and $Y_\zeta(\omega)$ are frequency-dependent linear-response vectors and the perturbation $\mu_{\zeta,ai} = \langle\phi_a|\hat{\mu}_\zeta|\phi_i\rangle$. Considering a global hybrid XC functional with an amount a_x of the Fock exchange, **A** and **B** supermatrix elements are defined as

$$A_{ia,jb} = \delta_{ij}\delta_{ab}(\epsilon_a - \epsilon_i) + 2(ia|jb) - a_x(ij|ab) + (1 - a_x)(ia|f_{XC}|jb) \tag{2}$$

and

$$B_{ia,jb} = 2(ia|bj) - a_x(ib|aj) + (1 - a_x)(ia|f_{XC}|bj) \tag{3}$$

For an excited-state calculation, the perturbation is set to 0, and excited-state energies (ω_n) and their single-(de)excitation eigenvectors ($\mathbf{X}_n$ and $\mathbf{Y}_n$) are determined. Note that for small-gap systems, undesired complex roots may appear in the solution of eq 1 (with the perturbation set to 0), making the computation of σ_{2PA} impossible. Solving this problem efficiently will be the subject of future studies.

In the sTD-DFT formalism,[65−70] three approximations are applied to the linear-response TD-DFT eq 1. The first approximation neglects $(ia|f_{XC}|jb)$ and $(ia|f_{XC}|bj)$ responses of the XC functional. In the second one, $(ia|jb)$, $(ia|bj)$, and $(ib|aj)$ exchange-type and $(ij|ab)$ Coulomb-type integrals are replaced by short-range damped Coulomb interactions of transition density monopoles according to

$$(pq|rs)' = \sum_A^N \sum_B^N q_{pq}^A q_{rs}^B \Gamma_{AB} \tag{4}$$

where q_{pq}^A are atom-centered transition charges determined by a Löwdin population analysis. The Mataga−Nishimoto−Ohno−Klopman (MNOK)[80−82] damped Coulomb operator for exchange integrals takes the form

$$\Gamma_{AB}^K = \left(\frac{1}{(R_{AB})^{y_K} + \eta^{-y_K}}\right)^{1/y_K}, \tag{5}$$

while for Coulomb integrals, it reads

$$\Gamma_{AB}^J = \left(\frac{1}{(R_{AB})^{y_J} + (a_x\eta)^{-y_J}}\right)^{1/y_J} \tag{6}$$

where y_K and y_J are globally fitted parameters for the whole range of a_x, R_{AB} is the interatomic distance, and η is the chemical hardness mean between atoms *A* and *B*. Considering

https://doi.org/10.1021/acs.jpca.2c02395
J. Phys. Chem. A 2022, 126, 7534−7547

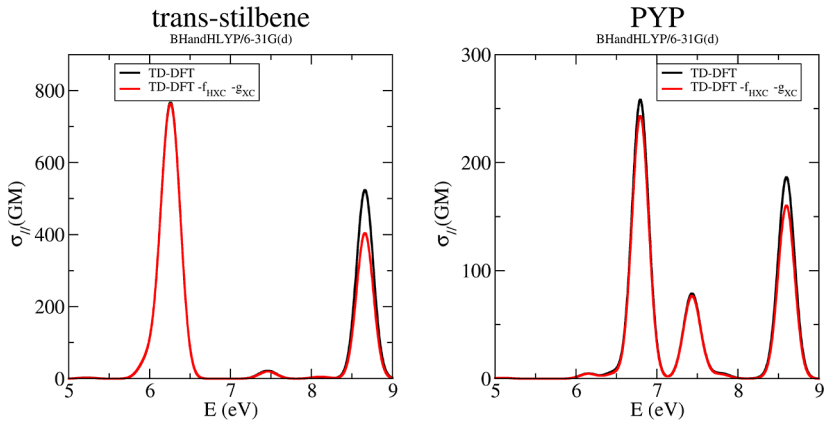

Figure 1. 2PA spectra of *trans*-stilbene and the PYP chromophore at the TD-DFT/BHandHLYP/6-31G(d) level with and without including the Hartree XC kernel as well as the XC functional kernel in the evaluation of 2PA cross-sections.

a hybrid XC functional, y_K and y_J are linear functions of the amount of the exact exchange a_x that were determined by a least-squares fit to reference excitations as $y_K = 1.42 + 0.48a_x$ and $y_J = 0.20 + 1.83a_x$, respectively.[65] The third approximation concerns the truncation of the space of singly excited configurations controlled by a single-energy threshold (E_{thresh}).

In the quadratic-response sTD-DFT formalism,[68] the first hyperpolarizability is obtained thanks to the frequency-dependent linear-response vectors $X_\zeta(\omega)$ and $Y_\zeta(\omega)$ as

$$\beta_{\xi\zeta\eta}(-2\omega;\ \omega,\ \omega) = A - B \tag{7}$$

$$A = \sum_{\text{perm.}\xi,\zeta,\eta} \left\{ \sum_{aij} X_{\xi,ai}(-2\omega)[-\mu_{\zeta,ij}]Y_{\eta,aj}(\omega) \right\} \tag{8}$$

$$B = \sum_{\text{perm.}\xi,\zeta,\eta} \left\{ \sum_{iab} X_{\xi,ai}(-2\omega)[-\mu_{\zeta,ab}]Y_{\eta,bi}(\omega) \right\} \tag{9}$$

where the permutations of ξ, ζ, and η Cartesian orientations and frequencies are included in both summations. This expression includes two additional approximations: the neglect of the XC functional kernel and the Hartree XC terms. Thus, only the unrelaxed first hyperpolarizability is evaluated at the sTD-DFT level. Note that we showed in ref 68 that for push−pull π-conjugated systems, these approximations do not have much impact on the frequency dispersion of β_{HRS}.

At the pole $2\omega = \omega_n$ of the quadratic response function, 2P transition moments $M_{\zeta\eta}^{0\to n}$ can be extracted from the single residue of the sTD-DFT quadratic response function

$$\lim_{2\omega\to\omega_n} (2\omega - \omega_n)\beta_{\xi\zeta\eta}(-2\omega;\ \omega,\ \omega) = -M_{\zeta\eta}^{0\to n}\langle 0|\mu_\zeta|n\rangle \tag{10}$$

$$M_{\zeta\eta}^{0\to n} = -A' + B' \tag{11}$$

where

$$A' = \sum_{\text{perm.}\xi,\zeta,n} \left\{ \sum_{aij} X_{n,ai}[-\mu_{\zeta,ij}(1 - \delta_{\zeta n})]Y_{\eta,aj}(\omega_n/2) \right\} \tag{12}$$

and

$$B' = \sum_{\text{perm.}\xi,\zeta,n} \left\{ \sum_{iab} X_{n,ai}[-\mu_{\zeta,ab}(1 - \delta_{\zeta n})]Y_{\eta,bi}(\omega_n/2) \right\} \tag{13}$$

$\delta_{\zeta n}$ is the Kronecker delta, meaning that the central term is 0 for the permutation with an excited state. As for the quadratic response function, 2P transition moments are unrelaxed due to the neglect of the Hartree XC kernel. Including it would result into additional approximations and parameterizations of four-center two-electron integrals that we would like to avoid. These approximations might introduce inconsistencies in the evaluation of the 2PA cross-sections as well as in (quasi-)energy derivatives and violation of sum rules. To assess the impact of such approximations on the evaluation of 2PA strengths, we computed for *trans*-stilbene and the PYP chromophore TD-DFT/BHandHLYP/6-31G(d) 2PA spectra with and without considering the neglect of XC functional kernel and the Hartree XC terms. These calculations were performed with a modified version of GAMESS.[83,84] Figure 1 shows these results. For both compounds, the impact of such approximations on the evaluation of 2PA cross-sections is rather small. This is an interesting finding that should be further assessed for a larger set of compounds in the future. In the sTD-DFT framework, we can probably admit that contributions to 2PA cross-sections from the Hartree XC and XC functional kernels should be below the intrinsic error of the method. Future works should confirm this statement.

The elements of the transition strength matrix are computed as products of 2P transition dipole moments as

$$S_{\zeta\eta,\xi\nu} = M_{\zeta\eta}^{0\to n} M_{\xi\nu}^{0\to n} \tag{14}$$

The rotationally averaged 2PA strength[85,86] is given by

$$\langle\delta^{2\text{PA}}\rangle = \frac{F}{30}\sum_{\zeta,\eta} S_{\zeta\zeta,\eta\eta} + \frac{G}{30}\sum_{\zeta,\eta} S_{\zeta\eta,\zeta\eta} + \frac{H}{30}\sum_{\zeta,\eta} S_{\zeta\eta,\eta\zeta} \tag{15}$$

where F, G, and H are parameters all equal 2 for parallel linearly polarized incident light. This quantity can be converted into the macroscopic 2PA cross-section as

$$\sigma^{2\text{PA}} = \frac{N\pi^3\alpha a_0^5(2\omega)^2}{c}\langle\delta^{2\text{PA}}\rangle S(2\omega,\ \omega_n,\ \Gamma) \tag{16}$$

where $N = 1$ for the degenerated case and $N = 2$ for a double-beam experiment accounting for the photon dissipation rate of

https://doi.org/10.1021/acs.jpca.2c02395
J. Phys. Chem. A 2022, 126, 7534−7547

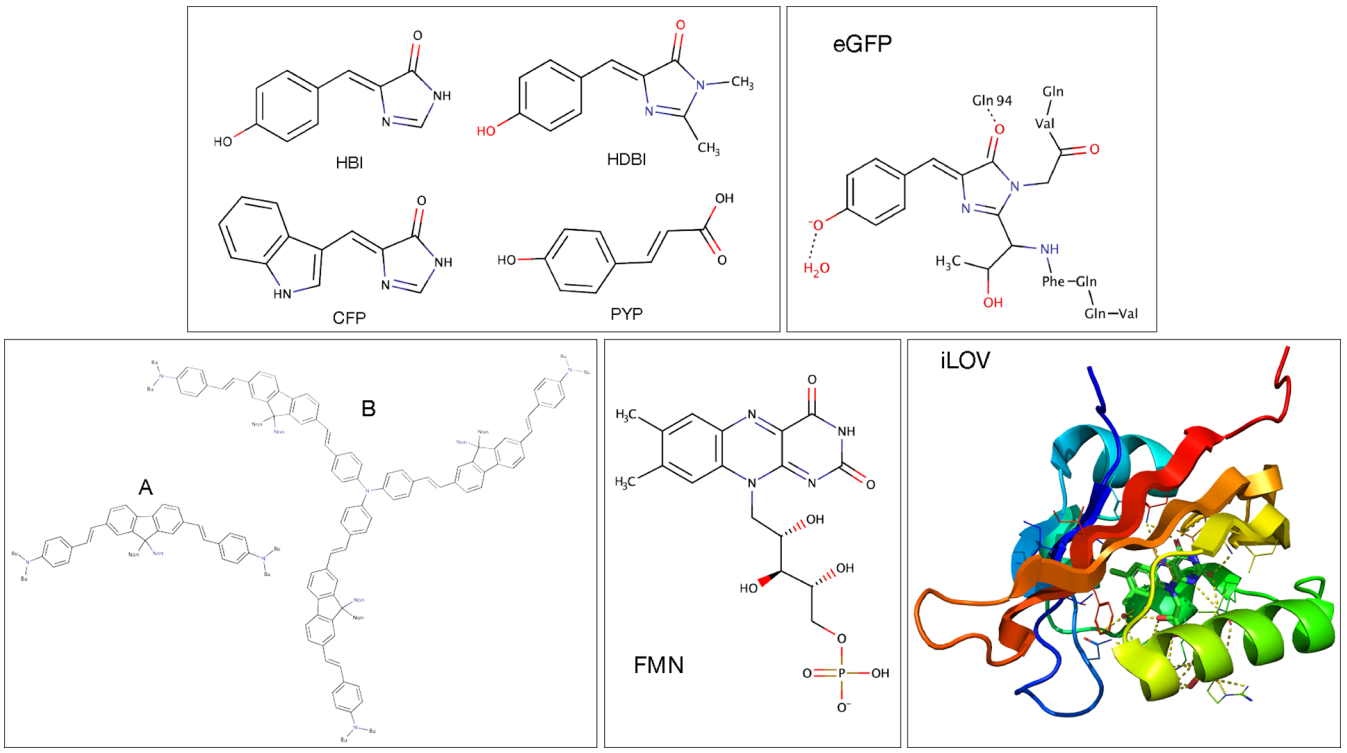

Figure 2. Chemical structures of considered systems: four FP chromophores (HBI, HBDI, CFP, and PYP), the eGFP chromophore with its first shell of residues, the quadrupolar chromophore (**A**) and its branched version (**B**), FMN, and the iLOV protein.

both laser beams,[32] α is the fine structure constant, a_0 is the Bohr radius, c is the speed of light, and $S(2\omega, \omega_n, \Gamma)$ is a line-shape function accounting for spectral broadening effects. Note that N needs to be multiplied by 4 if two times $M_{\zeta\eta}^{0\to n}$ is accounted for in the experimental definition considering the degenerated case.[32]

In the following, a Gaussian line shape is employed to compute 2PA spectra as it is usually used to compare with measurements in solution

$$G(2\omega, \omega_n, \Gamma) = \frac{\sqrt{\ln 2}}{\sqrt{\pi}\Gamma}\exp\left[-\ln 2\left(\frac{2\omega - \omega_n}{\Gamma}\right)^2\right] \quad (17)$$

where Γ is the half width at half-maximum. This function presents a maximum at $2\omega = \omega_n$ for which $G(\omega_n, \Gamma) = \frac{\sqrt{\ln 2}}{\sqrt{\pi}\Gamma}$. A Γ value of 0.1 eV is used throughout this study. Note that for gas-phase calculations, a Lorentzian line-shape function is usually employed.[32] Hence, the choice of the line-shape function represents some kind of (necessary) arbitrariness in the theoretical treatment.

The calculation of absolute 2PA cross-sections is a difficult task in quantum chemistry. First, an energy error in the excitation energy of a 2P transition impacts directly the σ^{2PA} value by its $(2\omega)^2$ dependence. Second, the choice of Γ strongly affects the cross-section. For example, going from a value of Γ = 0.1 to 0.2 eV decreases σ^{2PA} by a factor of 2. It is also unlikely that all 2P transitions for a given system inherit the same broadening as it is usually assumed.[21] In addition, the N parameter is sometimes difficult to determine from experimental details given in the literature. Hence, our calculations may provide only semiquantitative spectra and good trends among sets of molecules, but absolute σ^{2PA} are still difficult to assess a priori.

While our method allows the fast evaluation of 2PA cross-sections at a standard KS-DFT level of theory, the sTD-DFT implementation is also interfaced with the semiempirical sTD-DFT-xTB method[67] where the KS orbitals and their energies are replaced with TB-approximated ones, enabling ultrafast computations for systems up to ∼5000 atoms.

Computational Details. The evaluation of σ_{2PA} at the sTD-DFT level of theory was recently implemented in a development version of the stda program[87] which is freely available.

The structure of *trans*-stilbene was taken from ref 20. Figure 2 shows all other structures considered in this study. FP chromophores (HBI, HBDI, CFP, and PYP) were taken from the study of Beerepoot et al.[32] and were originally optimized by Nanda and Krylov[19] and Salem and Brown.[56] The eGFP chromophore and its first shell of surrounding residues was taken from ref 88. The quadrupolar chromophore (**A**) and its branched version (**B**)[72] were optimized at the ωB97X-D3/6-311G(d) level of theory. The negatively charged FMN chromophore was extracted from the iLOV X-ray structure that was previously used to model its second-harmonic generation.[64] The CREST[89] code was used to sample the conformational space with the GFN2-xTB method[90] considering water as a solvent with the GBSA model.[91] The 37 lowest-energy conformers were selected and optimized at the ωB97X-D/6-31G(d)/IEFPCM level of theory with water as a solvent. Free energies were computed including the solvent effects; zero-point energy; and translational, rotational, and vibrational contributions calculated at the same level. Boltzmann weights were obtained at 298.15 K. We selected the eight lowest-free-energy conformers contributing to 97.9% of the population at this temperature. These calculations for FMN were done with the Gaussian 16 A03 package[92] and the xtb 6.2.2 program.[93,94] The optimized structure of iLOV was

https://doi.org/10.1021/acs.jpca.2c02395
J. Phys. Chem. A 2022, 126, 7534−7547

taken from the study of Beaujean et al.[64] where the full protein including explicit surrounding water molecules was optimized at the ONIOM ωB97X-D3/6-31G(d):GFN2-xTB/GBSA-(water) level.

For *trans*-stilbene, the reference EOM-EE-CCSD/d-aug(-d)-cc-pVDZ ("-d" means that a set of d-functions were removed from the d-aug set) 2PA spectrum was taken from ref 20. For the set of FP chromophores, RI-CC2/d-aug(-d)-cc-pVDZ or aug-cc-pVDZ and CAM-B3LYP/6-31+G(d) first excitation energies and $\langle\delta^{2PA}\rangle$ were taken from ref 32 and EOM-EE-CCSD/d-aug(-d)-cc-pVDZ results for HBDI and PYP from the study of Nanda and Krylov.[19] In both cases, we computed the 20 first singlet excited states and their 2PA strengths with BHandHLYP for *trans*-stilbene and with both B3LYP and CAM-B3LYP XC functionals with the 6-31+G(d) basis set for FPs' chromophores using Dalton2018.0.[95,96] sTD-DFT calculations were performed using the same basis set and XC functionals. CAM-B3LYP default sTD-DFT parameters (a_x = 0.38, y_K = 0.9, and y_J = 1.86) were those advised by Risthaus et al.[97] Regarding eGFP, the experimental 2PA spectrum was taken from the study of Drobizhev et al.[4] The sTD-DFT-xTB method was used to compute the 2PA spectrum using default parameters. Considering **A** and **B**, their 2PA spectra in toluene were taken from the study of Blanchard-Desce and co-workers.[72] We computed their 2PA spectra at both sBHandHLYP[a]/6-31+G(d) and sTD-DFT-xTB levels using default parameters. The FMN 2PA spectra were measured in water by Homans et al.[73] and List et al.[30] The sTD-DFT-xTB method was used to compute 2PA spectra for the eight lowest-energy conformers of FMN using default parameters. The Boltzmann-averaged 2PA spectrum was also calculated. The 2PA spectrum of iLOV was computed at the sTD-DFT-xTB/GBSA(water) level of theory using default parameters considering the entire system and compared to the spectrum measured by Homans et al.[73]

DFT molecular orbitals and their energies were computed with Q-Chem 5.1[98] as input for sTD-DFT calculations using the stda program.[87] Geometry optimizations of **A** and **B** at the ωB97X-D3/6-311G(d) level of theory were also performed with Q-Chem 5.1.[98] $\langle\delta^{2PA}\rangle$ are given in atomic units while σ_{2PA} in Göppert-Mayer (GM).

RESULTS AND DISCUSSION

***trans*-Stilbene.** Figure 3 shows the reference EOM-EE-CCSD 2PA spectrum of *trans*-stilbene[20] as well as both TD-DFT and sTD-DFT BHandHLYP ones. In the reference spectrum, two main peaks are present mainly due to transitions from the ground 1^1A_g state to the 3^1A_g and 5^1A_g excited states at 5.74 and 6.28 eV, respectively. An excited-state analysis[20,21] reveals that both excited states are of mixed valence and $\pi \rightarrow p$ Rydberg character. Note that the 4^1A_g excited state also contributes to the second peak. Table 1 shows excitation energies and 2PA strengths for the four first excited states of the A_g irrep obtained at all these levels of theory. The first observation regarding TD-DFT results with respect to the EOM-EE-CCSD ones is the decrease in energy difference between 3^1A_g and 5^1A_g excited-state energies from 0.54 to 0.27 (0.29) eV at BHandHLYP/d-aug-cc-pVDZ (6-31+G(d)) levels, leading to the disappearance of the first peak. The second one is the energy shift of −0.19 (−0.29) eV for the 5^1A_g state when described at the TD-DFT level with both d-aug-cc-pVDZ and 6-31+G(d) basis sets in comparison to the EOM-EE-CCSD excitation energy. Regarding 2PA strengths,

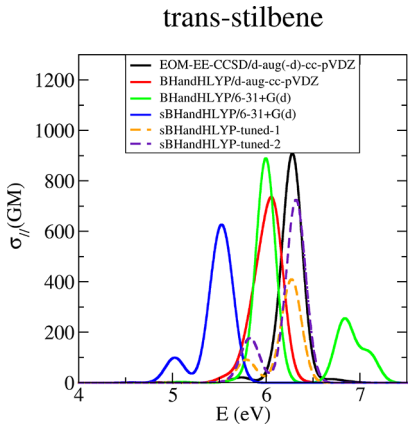

Figure 3. 2PA spectra of *trans*-stilbene at EOM-EE-CCSD/d-aug(-d)-cc-pVDZ, BHandHLYP/d-aug-cc-pVDZ, and BHandHLYP/6-31+G(d) levels of theory as well as with the sBHandHLYP/6-31+G(d) method using default parameterization, y_K = 0.9 and y_J = 0.7 (tuned-1) and y_K = 0.1 and y_J = 0.7 (tuned-2) parameters considering E_{thresh} = 9 eV, N = 1, and Γ = 0.1 eV.

Table 1. Excitation Energies and 2PA Strengths for the Four First Excited States of *trans*-Stilbene Belonging to the Totally Symmetric Representation of the C_{2h} Point Group at EOM-EE-CCSD/d-aug(-d)-cc-pVDZ, BHandHLYP/d-aug-cc-pVDZ, and BHandHLYP/6-31+G(d) Levels of Theory as Well as with the sBHandHLYP/6-31+G(d) Method Using Default Parameterization, y_K = 0.9 and y_J = 0.7 (Tuned-1) and y_K = 0.1 and y_J = 0.7 (Tuned-2) Parameters Considering E_{thresh} = 9 eV

	EOM-EE-CCSD/ d-aug(-d)-cc-pVDZ		BHandHLYP/ d-aug-cc-pVDZ		BHandHLYP/ 6-31+G(d)	
states	ΔE (eV)	$\langle\delta^{2PA}\rangle$ (au)	ΔE (eV)	$\langle\delta^{2PA}\rangle$ (au)	ΔE (eV)	$\langle\delta^{2PA}\rangle$ (au)
2^1A_g	4.81	201	5.58	1240	5.09	2770
3^1A_g	5.74	1055	5.82	7930	5.70	7160
4^1A_g	6.15	3949	5.95	15,900	6.02	2310
5^1A_g	6.28	40,786	6.09	28,800	5.99	43,500
	sBHandHLYP/ 6-31+G(d)		sBHandHLYP tuned-1/6-31+G(d)		sBHandHLYP tuned-2/6-31+G(d)	
states	ΔE (eV)	$\langle\delta^{2PA}\rangle$ (au)	ΔE (eV)	$\langle\delta^{2PA}\rangle$ (au)	ΔE (eV)	$\langle\delta^{2PA}\rangle$ (au)
2^1A_g	4.59	181	5.47	125	5.50	175
3^1A_g	5.01	5920	5.78	5010	5.82	9601
4^1A_g	5.42	14,888	6.20	2999	6.26	1515
5^1A_g	5.54	28,828	6.28	16,988	6.32	32,349

BHandHLYP/d-aug-cc-pVDZ (6-31+G(d)) $\langle\delta^{2PA}\rangle$ for the 5^1A_g state is 6.7% (29.4%) larger (smaller) with respect to the EOM-CCSD one, while $\langle\delta^{2PA}\rangle$ for lower-energy states are badly described.

Using the sTD-DFT method with the default parameters restores the energy difference between 3^1A_g and 5^1A_g states to 0.53 eV, only 0.01 eV away from the EOM-EE-CCSD result. However, the sBHandHLYP 5^1A_g excitation energy is red-shifted by 0.74 eV with respect to the EOM-CCSD one. 2^1A_g $\langle\delta^{2PA}\rangle$ drastically improves with respect to the full TD-DFT scheme with only 10.0% underestimation in comparison with the reference, while it was 14 times higher with TD-DFT. Its excitation energy is also not so far from the reference, while higher-energy excitations are systematically underestimated. The global shape of the sBHandHLYP 2PA spectrum is better

https://doi.org/10.1021/acs.jpca.2c02395
J. Phys. Chem. A 2022, 126, 7534−7547

that of the full scheme, but the spectrum is globally red-shifted with respect to EOM-CCSD and TD-DFT ones. The observed energy red shift is typical of the sTD-DFT method used with the BHandHLYP XC functional. Note that $\langle\delta^{2PA}\rangle$ for the 3^1A_g state is still 5.6 times too large in comparison to the EOM-CCSD one and 5^1A_g $\langle\delta^{2PA}\rangle$ is 29.3% lower. Thus, 3^1A_g and 4^1A_g states at the sBHandHLYP level are as badly treated as with regular TD-DFT. The 2^1A_g excitation energy and $\langle\delta^{2PA}\rangle$ are improved, while the 5^1A_g excitation energy is underestimated with respect to the reference, and its $\langle\delta^{2PA}\rangle$ remains within the same order of magnitude as the BHandHLYP/d-aug-cc-pVDZ value.

For *trans*-stilbene, all 2P-active states are one-photon absorption (1PA) dark states because of symmetry. Note that the performance of the sTD-DFT method in characterizing dark states has never been investigated and that the method was primarily parameterized for 1P-active states. Thus, the current parameterization may not be suited for 2P excitations. It is always possible to refit the sTD-DFT integral parameters for a particular compound, reproducing a reference calculation, using the sTD-DFT scheme as a model. However, this approach presents limitations and cannot cure all sTD-DFT deficiencies. As an illustration, we explored different sets of parameters to observe how they impact comparisons with respect to reference calculations. We first propose to use y_K = 0.9 and y_J = 0.7 instead of y_K = 1.66 and y_J = 1.115 default parameters. This change of parameters unfortunately shifts the 2^1A_g excitation energy to a higher energy with a 0.66 eV difference with respect to the EOM-CCSD value, while 3^1A_g, 4^1A_g, and 5^1A_g excitation energies are less than 0.05 eV away from those of the reference. A relatively good energy splitting between 3^1A_g and 5^1A_g states is maintained with a difference of 0.49 eV. Regarding $\langle\delta^{2PA}\rangle$, 3^1A_g states remain as badly described as before the change of parameters. The 4^1A_g 2PA strength is drastically improved with a value of 24.1% lower with respect to the reference. 5^1A_g $\langle\delta^{2PA}\rangle$ is 58.3% lower with respect to the EOM-CCSD cross-section, while it was 29.3% lower with the default parameterization. With this first set of parameters, excitation energies are drastically improved except for 2^1A_g. Only 4^1A_g $\langle\delta^{2PA}\rangle$ is improved, while 2^1A_g and 5^1A_g ones are better described with default parameters.

Further decreasing the y_K parameter to 0.1 does not drastically change excitation energy positions but strongly improves 5^1A_g and 2^1A_g $\langle\delta^{2PA}\rangle$ with 20.7 and 19.9% differences with respect to reference values, respectively. However, the 3^1A_g 2PA value increases drastically, while the 4^1A_g 2PA strength is now 61.6% below the reference. Note that these new sets of parameters also help better reproduce the EOM-CCSD 1PA spectra as shown in Figure 4. Adjusting parameters is not a miracle cure for the sTD-DFT method. It cannot heal TD-DFT deficiencies like for the description of the 3^1A_g state. It could help improve the excitation energy and 2PA strength for one transition in particular but could also spoil the nature of the excited states concerned. Therefore, changing parameters should be done very carefully. Nonetheless, *trans*-stilbene remains the worst-case scenario for our method with the Rydberg character of its 2P-active states that are quite difficult to handle by our semiempirical integrals.

FP Chromophores. Table 2 shows excitation energies and 2PA strengths for the lowest-energy excited state of the four FP chromophores belonging to the C_s point group. Note that for the *para*-coumaric acid (PYP chromophore), the first A′ excited state at both RI-CC2 and TD-DFT levels is the second

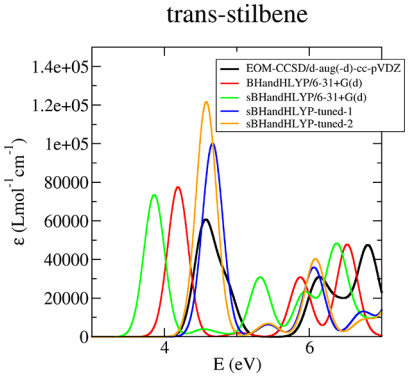

Figure 4. 1PA spectra of *trans*-stilbene at EOM-EE-CCSD/d-aug(-d)-cc-pVDZ and BHandHLYP/6-31+G(d) levels of theory as well as with the sBHandHLYP/6-31+G(d) method using default parameterization, y_K = 0.9 and y_J = 0.7 (tuned-1) and y_K = 0.1 and y_J = 0.7 (tuned-2) parameters considering E_{thresh} = 9 eV.

one in the EOM-EE-CCSD calculation.[32] For HBI, with deviations from the CC2 excitation energy of −0.20 and 0.02 eV for B3LYP and CAM-B3LYP, respectively, CAM-B3LYP provides the best result. In both cases, 2PA strengths are around a third of the CC2 value. Beerepoot et al.[32] already pointed out this behavior for CAM-B3LYP 2PA strengths where they linked it to underestimated excited-state dipole moments at this level. Using default sTD-DFT parameters for both XC functionals, sTD-DFT excitation energies are not so far from those obtained with the full scheme. However, their 2PA strengths differ largely by 100.0% for B3LYP and 25.0% with CAM-B3LYP. These differences are linked to inherent approximations in the sTD-DFT scheme. In particular, the fact that we are comparing relaxed TD-DFT 2PA strengths to unrelaxed sTD-DFT ones. Note that sB3LYP $\langle\delta^{2PA}\rangle$ is closer to the CC2 reference value. As pointed out for *trans*-stilbene, it is always possible to reparameterize the sTD-DFT integrals to better fit a reference using the sTD-DFT method as a model to screen sets of similar compounds. However, this approach is only valid when reference calculations are available. On the contrary, only default parameters can be used. To best reproduce the CC2 values for HBI, we used y_K = 0.2 and y_J = 0.35 instead of y_K = 1.516 and y_J = 0.566 for B3LYP and y_K = 0.1 and y_J = 1.5 instead of y_K = 0.9 and y_J = 1.86 for CAM-B3LYP. These changes of parameters close the gap with the CC2 excitation energy with differences not greater than 0.01 eV. They also largely improve 2PA strengths where the sB3LYP one is only 7.5% lower than the reference value, but still 52.0% deviation is observed when using CAM-B3LYP. In both cases, our "fitted" values are obviously better than those provided by regular TD-DFT because they were especially adjusted for. Next, we assess how the refitted sTD-DFT scheme deals with similar compounds.

For HBDI, similar trends are observed. With both reparameterized sB3LYP and sCAM-B3LYP schemes, sTD-DFT values compare best with the CC2 reference than the full scheme, showing that the addition of two methyl groups does not impair the treatment. Note that B3LYP $\langle\delta^{2PA}\rangle$ is slightly nearer the EOM-EE-CCSD one than with the simplified method, but the fine-tuned sCAM-B3LYP values still provide the best agreement. With a more drastic change in the structure with respect to HBI, results for CFP and PYP still present similar trends. Excitation energies using fine-tuned parameters are improved with respect to references as well as

https://doi.org/10.1021/acs.jpca.2c02395
J. Phys. Chem. A 2022, 126, 7534−7547

Table 2. Excitation Energies and 2PA Strengths for HBI, HBDI, CFP, and PYP at EOM-EE-CCSD/d-aug(-d)-cc-pVDZ from the Study of Nanda and Krylov[19] When Available, RI-CC2/d-aug(-d)-cc-pVDZ or aug-cc-pVDZ and CAM-B3LYP/6-31+G(d) from the Study of Beerepoot et al.,[32] and B3LYP/6-31+G(d) Levels of Theory as Well as with sB3LYP/6-31+G(d) and sCAM-B3LYP/6-31+G(d) Schemes Using Default Parameterizations and Fine-Tuned Parameters Considering E_{thresh} = 9 eV

	method	basis set	parameters	ΔE (eV)	$\langle\delta^{2PA}\rangle$ (au)
HBI	RI-CC2[32]	d-aug(-d)-cc-pVDZ		3.70	3345
	B3LYP	6-31+G(d)		3.50	962
	sB3LYP	6-31+G(d)	default (y_K = 1.516 y_J = 0.566)	3.46	1931
	sB3LYP	6-31+G(d)	y_K = 0.2 y_J = 0.35	3.70	3095
	CAM-B3LYP[32]	6-31+G(d)		3.72	1057
	sCAM-B3LYP	6-31+G(d)	default (y_K = 0.9 y_J = 1.86)	3.65	796
	sCAM-B3LYP	6-31+G(d)	y_K = 0.1 y_J = 1.5	3.71	1604
HBDI	EOM-EE-CCSD[19]	d-aug(-d)-cc-pVDZ		3.97	978
	RI-CC2[32]	d-aug(-d)-cc-pVDZ		3.69	1135
	B3LYP	6-31+G(d)		3.50	370
	sB3LYP	6-31+G(d)	default (y_K = 1.516 y_J = 0.566)	3.43	361
	sB3LYP	6-31+G(d)	y_K = 0.2 y_J = 0.35	3.71	1696
	CAM-B3LYP[32]	6-31+G(d)		3.73	516
	sCAM-B3LYP	6-31+G(d)	default (y_K = 0.9 y_J = 1.86)	3.65	310
	sCAM-B3LYP	6-31+G(d)	y_K = 0.1 y_J = 1.5	3.73	840
CFP	RI-CC2[32]	aug-cc-pVDZ		3.49	5197
	B3LYP	6-31+G(d)		3.31	2120
	sB3LYP	6-31+G(d)	default (y_K = 1.516 y_J = 0.566)	3.24	4557
	sB3LYP	6-31+G(d)	y_K = 0.2 y_J = 0.35	3.52	4741
	CAM-B3LYP[32]	6-31+G(d)		3.55	1674
	sCAM-B3LYP	6-31+G(d)	default (y_K = 0.9 y_J = 1.86)	3.45	1743
	sCAM-B3LYP	6-31+G(d)	y_K = 0.1 y_J = 1.5	3.52	2445
PYP	EOM-EE-CCSD[19]	d-aug(-d)-cc-pVDZ		4.75	2631
	RI-CC2[32]	d-aug(-d)-cc-pVDZ		4.37	3281
	B3LYP	6-31+G(d)		4.08	2560
	sB3LYP	6-31+G(d)	default (y_K = 1.516 y_J = 0.566)	4.07	3133
	sB3LYP	6-31+G(d)	y_K = 0.2 y_J = 0.35	4.38	4805
	CAM-B3LYP[32]	6-31+G(d)		4.36	1953
	sCAM-B3LYP	6-31+G(d)	default (y_K = 0.9 y_J = 1.86)	4.43	1175
	sCAM-B3LYP	6-31+G(d)	y_K = 0.1 y_J = 1.5	4.53	2214

$\langle\delta^{2PA}\rangle$ except for PYP using the B3LYP XC functional. Note that the PYP structure has no imidazolinone ring. This possibly explains the discrepancy, showing the limitation of parameter tuning when the compound becomes too much structurally different. Note that while the other chromophores are taken from GFP-like proteins, this is not the case for the PYP chromophore. This illustrates that refitting the sTD-DFT method for special-purpose applications, for example, the screening of rather similar systems, might be interesting but should be carefully done. Here, only reference data are available for the first excited state of this set of molecules. Thus, we do not know the impact of such refits on other 2P-active states. As already stated before, this is not a miracle cure, and when the compound becomes structurally different, as is the case with PYP here, the parameter tuning approach presents limitations.

For the sake of completeness, Figure 5 shows TD-DFT and sTD-DFT (default parameters) 2PA spectra for these FP chromophores using CAM-B3LYP/6-31+G(d). Global TD-DFT spectral shapes are more or less well reproduced by the simplified scheme, while 2PA cross-sections for the largest intensities are overestimated for HBI, HBDI, and CFP and underestimated for PYP. In the case of CFP, we clearly observe that at higher energies, stick spectra are not completely equivalent. Note that we did not compare spectral shapes at higher levels of theory because these data are not available in refs 19 and 32 where only the 2PA cross-sections for the first excited state are available.

One important feature of our implementation is the drastic cut in computational costs with respect to those of the TD-DFT. For this set of molecules, Figure 6a,b shows the convergence of 2PA strengths and excitation energies as a function of the single-excitation energy selection threshold that controls the truncation of the response expansion space in sTD-DFT. These results show fast convergence for both quantities with E_{thresh}, while trends are maintained for the whole range of values considered. 2PA strengths at E_{thresh} = 7 eV are between 40 and 46%, too large with respect to values at 15 eV. At E_{thresh} = 9 eV, these discrepancies diminish to 9−22%. The excitation energies converge faster as a function of cut-off with less than 2% overestimation with E_{thresh} = 7 eV. Figure 6c also shows CPU times on an eight-core desktop computer (Intel core i7-6700, 3.40 GHz) with the stda program[87] as a function of E_{thresh} for this set of molecules. TD-DFT CPU times on 28 CPUs (Intel Xeon CPU E5-2660 v4, 3.2 GHz) using Dalton2018.0[95,96] are also provided to

https://doi.org/10.1021/acs.jpca.2c02395
J. Phys. Chem. A 2022, 126, 7534−7547

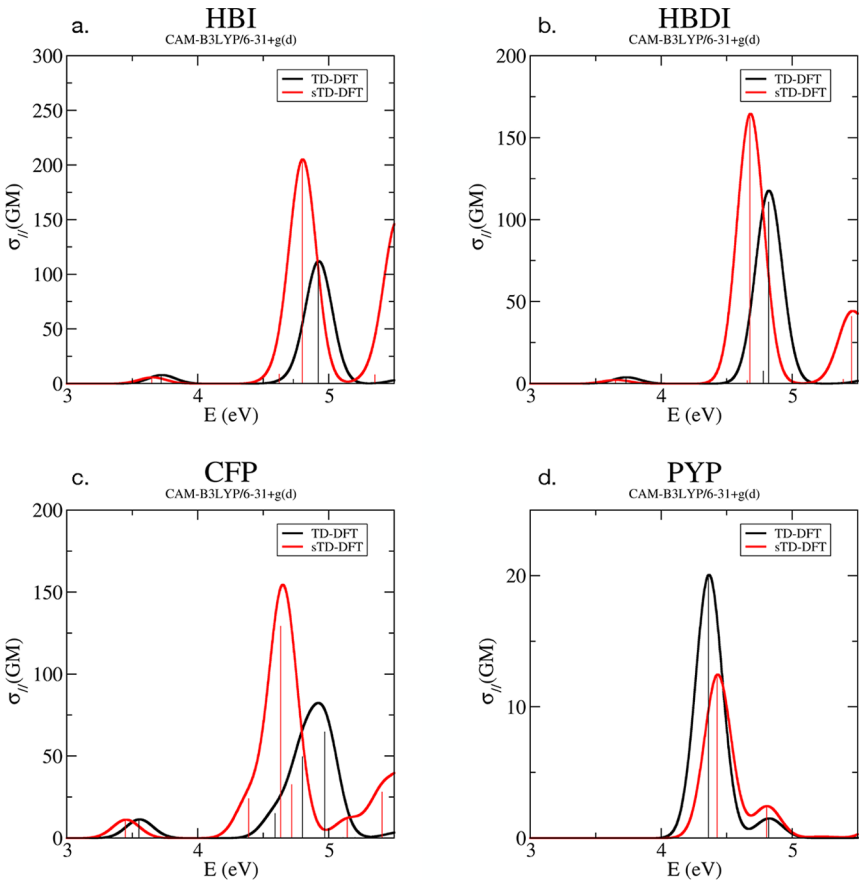

Figure 5. 2PA spectra for HBI (a), HBDI (b), CFP (c), and PYP (d) evaluated at both TD-DFT and sTD-DFT levels of theory with the CAM-B3LYP XC functional and 6-31+G(d) basis set considering Γ = 0.1 eV and N = 1.

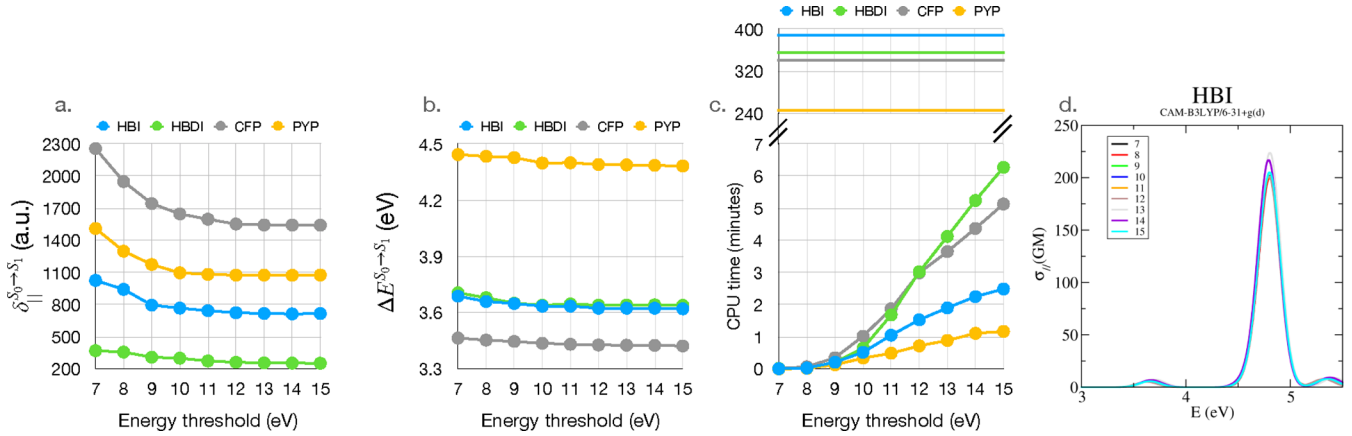

Figure 6. sCAM-B3LYP/6-31+G(d) 2PA strengths (a) and excitation energies (b) for the first excited state of HBI, HBDI, CFP, and PYP as a function of the single-energy threshold. CPU times (c) are also provided for sCAM-B3LYP calculations (dotted lines) performed on eight-core desktop computers (Intel core i7-6700, 3.40 GHz) with the stda program,[87] while full calculations to compute 20 excited states (plain lines) were done on 28 CPUs (Intel Xeon CPU E5-2660 v4, 3.2 GHz) using Dalton2018.0.[95,96] 2PA sCAM-B3LYP spectra for HBI (d) evaluated for the same range of energy thresholds considering Γ = 0.1 eV and N = 1.

compute the 20 first excited states: 388 (HBI), 356 (HBDI), 341 (CFP), and 246 min (PYP). Values computed are obtained in less than 2 s for E_{thresh} = 7 eV and 21 s for 9 eV. The longest computation time is observed for HBDI with about 6 min at an energy threshold of 15 eV. With E_{thresh} = 7 eV, the sTD-DFT 2PA calculations are about 20,000 times faster than the TD-DFT ones. This reduces by 300 times for E_{thresh} = 10 eV while drastically improving the convergence of 2PA strengths. As shown in Figure 6d, the global shape of the 2PA spectrum of HBI is not much influenced by the change in E_{thresh}.

eGFP. As a first step toward the simulation of the 2PA of FPs, we use eGFP's deprotonated chromophore and its first shell of surrounding residues and water molecules (359 atoms). This model was already successfully used to evaluate the second-harmonic generation of eGFP at both ONIOM

https://doi.org/10.1021/acs.jpca.2c02395
J. Phys. Chem. A 2022, 126, 7534−7547

MP2:HF/6-31+G(d) and sTD-DFT-xTB levels of theory.[68,88] Figure 7 compares the experimental 2PA spectrum

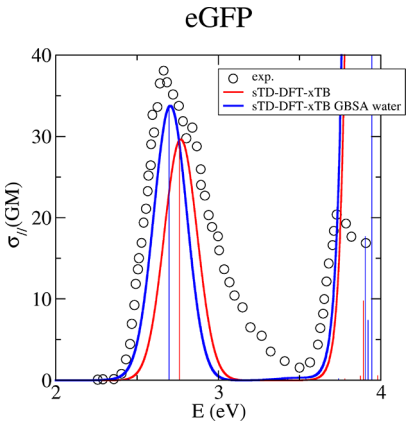

Figure 7. Experimental 2PA spectrum measured by Drobizhev et al.[4] in comparison with that from the sTD-DFT-xTB computed for E_{thresh} = 7 eV, Γ = 0.1 eV, and N = 2 with and without solvent effects using the GBSA model with water as a solvent.

obtained by Drobizhev et al.[4] to that computed at the sTD-DFT-xTB level of theory with E_{thresh} = 7 eV and N = 2. Note that sTD-DFT-xTB default parameters are used. The sTD-DFT calculation without solvent effects took 45 s of CPU time (8 Intel cores i7-6700, 3.40 GHz). Without any applied empirical spectral shift, the comparison with the experimental spectrum is striking. The main peak is due to the lowest-energy excited state with an excitation energy of 2.76 eV and a 2PA cross-section of 30 GM computed with the sTD-DFT-xTB method and 2.70 eV and 34 GM when accounting for solvent effects. These values are close to those measured by Drobizhev et al.:[4] 2.68 eV and 39 GM, which is very encouraging for such a rather complex system.

Quadrupolar Chromophore and Its Branched Version. Figure 8 compares the experimental 2PA spectra for the quadrupolar chromophore **A** and its branched version **B** to sBHandHLYP/6-31+G(d) and sTD-DFT-xTB ones where energy corrections of −0.65 and −1.5 eV, respectively, are applied to account for missing solvatochromic effects. Experimentally, the peak observed at 3.35 eV with a σ^{2PA} of 1126 GM is enhanced to a value of 3700 GM for its branched trimer, while the excitation energy remains unchanged.[72] For **A**, by also applying an energy correction to the $(2\omega)^2$ contribution to σ^{2PA}, a value of 1334 GM was computed at the sBHandHLYP level for a (shifted) excitation energy at 3.41 eV, well-reproducing the experimental peak. From inspection of the natural transition orbitals, this transition has a charge transfer (CT) character. Going to the branched trimer **B**, the experimental enhancement by a factor of 3.3 is underestimated by the sBHandHLYP calculation to 1.34 while red-shifted by 0.24 eV. No energy shift is experimentally observed. The observed discrepancies for the branched chromophore at the sBHandHLYP level might be due to missing contributions from other conformers that are not included. To solve this, one should sample the conformer space for the branched chromophore and do extra 2PA calculations for each conformer. Then, a Boltzmann-averaged 2PA spectrum could be provided. At the sTD-DFT-xTB level, while the 2PA spectrum of **A** is well reproduced, the method failed to correctly describe σ^{2PA} of this CT transition of **B**.

FMN and iLOV. Table 3 shows excitation energies and 2PA strengths for lumiflavin (for which the FMN ribityl tail was replaced by a methyl group) at the CAM-B3LYP/cc-pVDZ+ level of theory obtained by List et al.[30] as well as for the lowest energy conformer of FMN with the sTD-DFT-xTB method. While these results seem very similar, the ribityl-5′-phosphate group in FMN plays a non-negligible part on the 2PA strengths because of the interaction of its phosphate end-group with isoalloxazine. This is confirmed by the sTD-DFT-xTB calculation on lumiflavin where 2PA responses are enhanced by a factor of 2.3. Figure 9 compares the experimental 2PA

Table 3. Excitation Energies and 2PA Strengths for Lumiflavin and FMN Obtained by List et al.[30] at the CAM-B3LYP/cc-pVDZ+ or PE-CAM-B3LYP Level of Theory as Well as with the sTD-DFT-xTB Method Considering E_{thresh} = 7 eV for the Lowest-Energy Conformer of FMN[a]

lumiflavin		FMN			
CAM-B3LYP		PE-CAM-B3LYP in water		sTD-DFT-xTB	
E (eV)	δ (au)	E (eV)	δ (au)	E (eV)	δ (au)
3.31	124	3.18 ± 0.06	177 ± 36	3.22	111
4.22	217	3.78 ± 0.10	415 ± 160	4.33	204

[a]The PE-CAM-B3LYP results were obtained for 50 configurations of FMN in aqueous solution.[30]

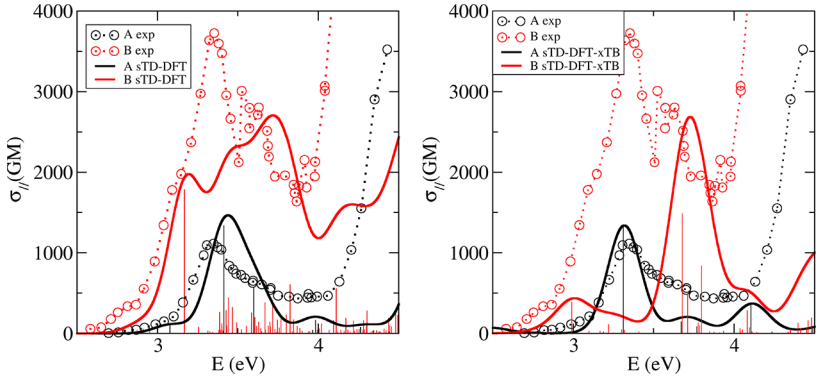

Figure 8. Experimental 2PA spectra for the quadrupolar chromophore **A** and its branched version **B**[72] as well as theoretical spectra obtained at both sBHanHLYP/6-31+G(d) and sTD-DFT-xTB levels of theory considering N = 1, Γ = 0.1 eV, E_{thresh} = 7 eV, and systematic energy shifts of −0.65 and −1.5 eV, respectively, for both methods.

https://doi.org/10.1021/acs.jpca.2c02395
J. Phys. Chem. A 2022, 126, 7534−7547

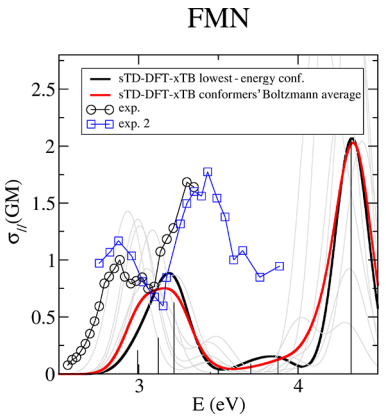

Figure 9. Experimental 2PA spectra of FMN in water solution from the study of Homans et al.[73] and List et al.[30] as well as theoretical spectra obtained at the sTD-DFT-xTB level of theory considering N = 1, Γ = 0.1 eV, and E_{thresh} = 7 eV for the eight lowest-energy conformers as well as the Boltzmann average for these conformers at 298.15 K.

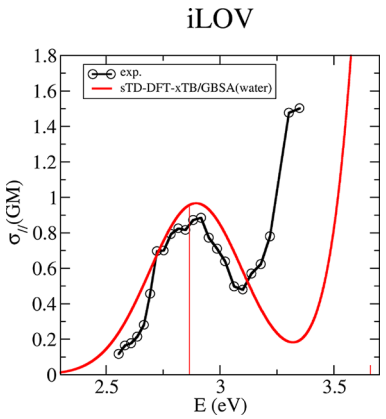

Figure 10. Experimental 2PA spectrum of iLOV from the study of Homans et al.[73] as well as the theoretical spectrum obtained at the sTD-DFT-xTB/GBSA(water) level of theory considering N = 1, E_{thresh} = 7 eV, and Γ = 0.2 eV.

spectra in water[30,73] for FMN with those of the lowest-energy conformer at the sTD-DFT-xTB level. The experimental 2PA cross-section of the first peak at 2.9 eV presents a value of around 1.0 GM to 1.2 GM according to refs 73 and 30. The sTD-DFT-xTB simulated peak presents a 2PA cross-section of 0.86 GM for which the excitation at 3.22 eV contributes to 0.63 GM. The rest of the contributions come from the broadening of a lower energy excitation at 3.12 eV with a 2PA cross-section of 0.31 GM. Experimentally, the energy difference between the two main peaks is 0.6 eV. This is overestimated by the sTD-DFT-xTB calculation in vacuum with a difference of 1.11 eV. A similar energy difference is observed for the CAM-B3LYP calculation on lumiflavin with 0.91 eV. List et al.[30] used quantum mechanics (QM)/molecular mechanics (MM) with PE to describe explicitly the impact of water solvent molecules on the 2PA response of FMN. For this, they took 50 configurations and computed excited states and 2PA strengths at the PE-CAM-B3LYP level of theory (see Table 3). They showed that the energy difference between both excited states with largest 2PA strengths decreases to a value of 0.60 eV as observed experimentally. Thus, to close the gap with respect to the experimental spectra, one should include explicitly solvent effects at the sTD-DFT-xTB and compute 2PA responses. This is out of the scope of the present work which is just showcasing the capabilities of the method. Figure 9 shows 2PA spectra at the sTD-DFT-xTB level for the eight lowest-energy conformers of FMN where the structural changes are due to rearrangements of the ribityl-5′-phosphate tail that is non-covalently interacting with isoalloxazine. The Boltzmann-averaged 2PA spectrum at 298.15 K for this set of conformers is also reported. The main difference with respect to the lowest-energy conformer 2PA spectrum is the broadening of the first peak that is enlarged as observed experimentally.

Finally, Figure 10 compares the experimental 2PA spectrum of iLOV from the study of Homans et al.[73] to the one computed at the sTD-DFT-xTB/GBSA(water) level of theory for the entire protein considering E_{thresh} = 7 eV. The calculation took 137 min on 28 CPUs (Intel Xeon CPU E5-2660 v4, 3.2 GHz) and only 0.87 min to compute the 20 first 2PA cross-sections after the excited-state calculation. To better fit the experimental peak, a Γ value of 0.2 eV is employed. This also compensates for the σ^{2PA} enhancement observed when accounting for equilibrium solvent effects with the GBSA model. Experimentally, the maximum of the first peak is located around 2.9 eV for iLOV. This is also the case for FMN in an aqueous solution. For iLOV, the agreement between the theory and experiment is striking even if the second peak (partially shown in Figure 9) is blue-shifted with respect to that from the experiment. Accounting explicitly for the protein surroundings around FMN provides the right red shift to reproduce the experimental result with respect to the FMN gas-phase calculation.

CONCLUSIONS

In this work, we derived the theoretical background for the evaluation of 2PA cross-sections in the framework of sTD-DFT. Computation of such a higher-order property is usually quite computationally involved and cannot be easily evaluated for large systems. With this new sTD-DFT implementation, we extend the reach of TD-DFT to ultralarge systems. Notwithstanding its computational efficiency, this new scheme inherits the pros and cons of TD-DFT. It is possible to reparameterize the two-electron integral parameters to better fit a reference, but this approach should be done carefully to avoid spoiling the nature of the excited states involved. Note that this is not a miracle cure for the sTD-DFT method, and this approach cannot solve all its deficiencies. In the absence of reference values, default parameters should be used as we did for the comparisons with the experimental values for the largest systems considered here. Note that we will introduce shortly a new scheme called eXact integral—sTD-DFT (XsTD-DFT) that avoids the use of semiempirical integrals and is a general solution to some inherent problems present in sTD-DFT, especially for 2PA cross-sections. The article should be submitted before the end of the current year. For this example, we illustrated the drastic cut of the computation times when using the sTD-DFT scheme with respect to TD-DFT. Considering a configuration selection threshold of 7 eV, the sTD-DFT 2PA calculations were at least 20,000 times faster for this set of FP chromophores.

Following this, we directly compared to experimental 2PA spectra those obtained with the sTD-DFT method for eGFP, a quadrupolar chromophore **A** and its branched version **B**, the FMN, and iLOV. Regarding eGFP, we used a model system of

https://doi.org/10.1021/acs.jpca.2c02395
J. Phys. Chem. A 2022, 126, 7534−7547

the chromophore cavity inside the protein, and we obtained an excellent agreement with the experimental values. In the case of **A** and **B**, sBHandHLYP 2PA spectra are in good agreement with those of the experiment, while the sTD-DFT-xTB method failed to describe the main CT excitation of **B**. We assessed dynamical structural effects for the rearrangement of the ribityl-5′-phosphate tail of FMN. The Boltzmann-averaged sTD-DFT-xTB 2PA spectrum presents a broadening of the first peak similar to that experimentally observed. Here, to close the gap with the experimental values, explicit water molecules should be included into the simulation as it was pointed out by List et al.[30] using QM/MM with PE.

Finally, to showcase the performance of the method and in particular of its sTD-DFT-xTB tight-binding version, the 2PA spectrum of the entire protein iLOV was computed and compared to that from the experiment. It was the opportunity to extend the all-atom quantum chemistry methodology we developed to evaluate the first hyperpolarizability[64] of FPs to 2PA. The striking agreement with the experimental results shows undoubtedly the relevance of such an approach. Such a methodology opens the way to a plethora of applications that could not be envisioned before, such as the design of new FPs with fine-tuned 2PA properties.

■ ASSOCIATED CONTENT

Supporting Information

The Supporting Information is available free of charge at https://pubs.acs.org/doi/10.1021/acs.jpca.2c02395.

Basis set effects for the first excitation energies and their 2PA strengths for the set of FP's chromophores and excitation energies, 2PA strengths, and 2PA cross-sections for eGFP, quadrupolar chromophore **A**, the branched chromophore **B**, and iLOV (PDF)

■ AUTHOR INFORMATION

Corresponding Author

Marc de Wergifosse − *Mulliken Center for Theoretical Chemistry, Institut für Physikalische und Theoretische Chemie der Universität Bonn, D-53115 Bonn, Germany;* orcid.org/0000-0002-9564-7303; Email: mdewergifosse@gmail.com

Authors

Pierre Beaujean − *Laboratory of Theoretical Chemistry, Unit of Theoretical and Structural Physical Chemistry, Namur Institute of Structured Matter, University of Namur, B-5000 Namur, Belgium;* orcid.org/0000-0003-3723-3257

Stefan Grimme − *Mulliken Center for Theoretical Chemistry, Institut für Physikalische und Theoretische Chemie der Universität Bonn, D-53115 Bonn, Germany;* orcid.org/0000-0002-5844-4371

Complete contact information is available at: https://pubs.acs.org/10.1021/acs.jpca.2c02395

Notes

The authors declare no competing financial interest.

■ ACKNOWLEDGMENTS

This work was supported by the DFG in the framework of the project "Theoretical studies of nonlinear optical properties of fluorescent proteins by novel low-cost quantum chemistry methods" (Nr. 450959503). Some of the calculations were performed on the computers of the Consortium des Équipements de Calcul Intensif, including those of the Technological Platform of High-Performance Computing, for which we gratefully acknowledge the financial support from the FNRS-FRFC, the Walloon Region, and the University of Namur (Convention nos. 2.5020.11, GEQ_U.G006.15, 1610468, and RW/GEQ2016).

■ ADDITIONAL NOTE

[a]s"functional name" is the short notation that refers to a sTD-DFT calculation made with this functional.

■ REFERENCES

(1) Göppert-Mayer, M.; Über, M. Über Elementarakte mit zwei Quantensprüngen. *Ann. Phys.* **1931**, *401*, 273−294.

(2) Denk, W.; Strickler, J. H.; Webb, W. W. Two-Photon Laser Scanning Fluorescence Microscopy. *Sci* **1990**, *248*, 73−76.

(3) Wang, B.-G.; König, K.; Halbhuber, K.-J. Two-Photon Microscopy of Deep Intravital Tissues and its Merits in Clinical Research. *J. Microsc.* **2010**, *238*, 1−20.

(4) Drobizhev, M.; Makarov, N. S.; Tillo, S. E.; Hughes, T. E.; Rebane, A. Two-Photon Absorption Properties of Fluorescent Proteins. *Nat. Methods* **2011**, *8*, 393−399.

(5) Streets, A. M.; Li, A.; Chen, T.; Huang, Y. Imaging without Fluorescence: Nonlinear Optical Microscopy for Quantitative Cellular Imaging. *Anal. Chem.* **2014**, *86*, 8506−8513.

(6) Kim, H. M.; Cho, B. R. Small-Molecule Two-Photon Probes for Bioimaging Applications. *Chem. Rev.* **2015**, *115*, 5014−5055.

(7) Parthenopoulos, D. A.; Rentzepis, P. M. Three-Dimensional Optical Storage Memory. *Sci* **1989**, *245*, 843−845.

(8) Dvornikov, A. S.; Walker, E. P.; Rentzepis, P. M. Two-Photon Three-Dimensional Optical Storage Memory. *J. Phys. Chem. A* **2009**, *113*, 13633−13644.

(9) Yu, J.; Cui, Y.; Wu, C.-D.; Yang, Y.; Chen, B.; Qian, G. Two-Photon Responsive Metal-Organic Framework. *J. Am. Chem. Soc.* **2015**, *137*, 4026−4029.

(10) Shao, B.; Baroncini, M.; Qian, H.; Bussotti, L.; Di Donato, M.; Credi, A.; Aprahamian, I. Solution and Solid-State Emission Toggling of a Photochromic Hydrazone. *J. Am. Chem. Soc.* **2018**, *140*, 12323−12327.

(11) Belfield, K. D.; Schafer, K. J.; Liu, Y.; Liu, J.; Ren, X.; Stryland, E. V. Multiphoton-Absorbing Organic Materials for Microfabrication, Emerging Optical Applications and Non-Destructive Three-Dimensional Imaging. *J. Phys. Org. Chem.* **2000**, *13*, 837−849.

(12) Carlotti, M.; Mattoli, V. Functional Materials for Two-Photon Polymerization in Microfabrication. *Small* **2019**, *15*, 1902687.

(13) Gao, D.; Agayan, R. R.; Xu, H.; Philbert, M. A.; Kopelman, R. Nanoparticles for Two-Photon Photodynamic Therapy in Living Cells. *Nano Lett.* **2006**, *6*, 2383−2386.

(14) Kim, S.; Ohulchanskyy, T. Y.; Pudavar, H. E.; Pandey, R. K.; Prasad, P. N. Organically Modified Silica Nanoparticles Co-encapsulating Photosensitizing Drug and Aggregation-Enhanced Two-Photon Absorbing Fluorescent Dye Aggregates for Two-Photon Photodynamic Therapy. *J. Am. Chem. Soc.* **2007**, *129*, 2669−2675.

(15) Shen, Y.; Shuhendler, A. J.; Ye, D.; Xu, J.-J.; Chen, H.-Y. Two-Photon Excitation Nanoparticles for Photodynamic Therapy. *Chem. Soc. Rev.* **2016**, *45*, 6725−6741.

(16) Zhou, Z.; Liu, J.; Huang, J.; Rees, T. W.; Wang, Y.; Wang, H.; Li, X.; Chao, H.; Stang, P. J. A self-assembled Ru-Pt metallacage as a lysosome-targeting photosensitizer for 2-photon photodynamic therapy. *Proc. Natl. Acad. Sci. U.S.A.* **2019**, *116*, 20296−20302.

(17) Sun, C.-L.; Li, J.; Wang, X.-Z.; Shen, R.; Liu, S.; Jiang, J.-Q.; Li, T.; Song, Q.-W.; Liao, Q.; Fu, H.-B.; et al. Rational Design of Organic Probes for Turn-On Two-Photon Excited Fluorescence Imaging and Photodynamic Therapy. *Chem* **2019**, *5*, 600−616.

(18) Helgaker, T.; Coriani, S.; Jørgensen, P.; Kristensen, K.; Olsen, J.; Ruud, K. Recent Advances in Wave Function-Based Methods of Molecular-Property Calculations. *Chem. Rev.* **2012**, *112*, 543−631.
(19) Nanda, K. D.; Krylov, A. I. Two-Photon Absorption Cross Sections within Equation-of-Motion Coupled-Cluster Formalism using Resolution-of-the-Identity and Cholesky Decomposition Representations: Theory, Implementation, and Benchmarks. *J. Chem. Phys.* **2015**, *142*, 064118.
(20) de Wergifosse, M.; Elles, C. G.; Krylov, A. I. Two-Photon Absorption Spectroscopy of Stilbene and Phenanthrene: Excited-State Analysis and Comparison With ethylene and Toluene. *J. Chem. Phys.* **2017**, *146*, 174102.
(21) de Wergifosse, M.; Houk, A. L.; Krylov, A. I.; Elles, C. G. Two-Photon Absorption Spectroscopy of trans-Stilbene, cis-Stilbene, and Phenanthrene: Theory and Experiment. *J. Chem. Phys.* **2017**, *146*, 144305.
(22) Nanda, K. D.; Krylov, A. I. The Effect of Polarizable Environment on Two-Photon Absorption Cross Sections Characterized by the Equation-of-Motion Coupled-Cluster Singles and Doubles Method Combined with the Effective Fragment Potential Approach. *J. Chem. Phys.* **2018**, *149*, 164109.
(23) Bhattacharyya, D.; Zhang, Y.; Elles, C. G.; Bradforth, S. E. Electronic Structure of Liquid Methanol and Ethanol from Polarization-Dependent Two-Photon Absorption Spectroscopy. *J. Phys. Chem. A* **2019**, *123*, 5789−5804.
(24) Bhattacharyya, D.; Zhang, Y.; Elles, C. G.; Bradforth, S. E. Electronic Structure of Liquid Alkanes: A Representative Case of Liquid Hexanes and Cyclohexane Studied Using Polarization-Dependent Two-Photon Absorption Spectroscopy. *J. Phys. Chem. A* **2021**, *125*, 7988−7999.
(25) Fu, M.; Wesolowski, T. A. The Challenge of Accurate Computation of Two-Photon Absorption Properties of Organic Chromophores in the Condensed Phase. *J. Chem. Theory Comput.* **2021**, *17*, 3652−3665.
(26) Hättig, C.; Christiansen, O.; Jo/rgensen, P. Coupled Cluster Response Calculations of Two-Photon Transition Probability Rate Constants for Helium, Neon and Argon. *J. Chem. Phys.* **1998**, *108*, 8355−8359.
(27) Paterson, M. J.; Christiansen, O.; Pawłowski, F.; Jørgensen, P.; Hättig, C.; Helgaker, T.; Sałek, P. Benchmarking Two-Photon Absorption with CC3 Quadratic Response Theory, and Comparison with Density-Functional Response Theory. *J. Chem. Phys.* **2006**, *124*, 054322.
(28) Friese, D. H.; Hättig, C.; Ruud, K. Calculation of Two-Photon Absorption Strengths with the Approximate Coupled Cluster Singles and Doubles Model CC2 using the Resolution-of-Identity Approximation. *Phys. Chem. Chem. Phys.* **2012**, *14*, 1175−1184.
(29) Sneskov, K.; Olsen, J. M. H.; Schwabe, T.; Hättig, C.; Christiansen, O.; Kongsted, J. Computational Screening of One- and Two-Photon Spectrally Tuned Channelrhodopsin Mutants. *Phys. Chem. Chem. Phys.* **2013**, *15*, 7567−7576.
(30) List, N. H.; Pimenta, F. M.; Holmegaard, L.; Jensen, R. L.; Etzerodt, M.; Schwabe, T.; Kongsted, J.; Ogilby, P. R.; Christiansen, O. Effect of chromophore encapsulation on linear and nonlinear optical properties: the case of "miniSOG", a protein-encased flavin. *Phys. Chem. Chem. Phys.* **2014**, *16*, 9950−9959.
(31) Beerepoot, M. T. P.; Friese, D. H.; Ruud, K. Intermolecular Charge Transfer Enhances Two-Photon Absorption in Yellow Fluorescent Protein. *Phys. Chem. Chem. Phys.* **2014**, *16*, 5958−5964.
(32) Beerepoot, M.; Friese, D.; List, N.; Kongsted, J.; Ruud, K. Benchmarking Two-Photon Absorption Cross Sections: Performance of CC2 and CAM-B3LYP. *Phys. Chem. Chem. Phys.* **2015**, *17*, 19306.
(33) Bednarska, J.; Zaleśny, R.; Tian, G.; Murugan, N. A.; Ågren, H.; Bartkowiak, W. Nonempirical Simulations of Inhomogeneous Broadening of Electronic Transitions in Solution: Predicting Band Shapes in One- and Two-Photon Absorption Spectra of Chalcones. *Molecules* **2017**, *22*, 1643.
(34) Beerepoot, M. T. P.; Alam, M. M.; Bednarska, J.; Bartkowiak, W.; Ruud, K.; Zaleśny, R. Benchmarking the Performance of Exchange-Correlation Functionals for Predicting Two-Photon Absorption Strengths. *J. Chem. Theory Comput.* **2018**, *14*, 3677−3685.
(35) Grabarek, D.; Andruniów, T. Assessment of Functionals for TDDFT Calculations of One- and Two-Photon Absorption Properties of Neutral and Anionic Fluorescent Proteins Chromophores. *J. Chem. Theory Comput.* **2019**, *15*, 490−508.
(36) Zaleśny, R.; Alam, M. M.; Day, P. N.; Nguyen, K. A.; Pachter, R.; Lim, C.-K.; Prasad, P. N.; Ågren, H. Computational Design of Two-Photon Active Organic Molecules for Infrared Responsive Materials. *J. Mater. Chem. C* **2020**, *8*, 9867−9873.
(37) Sałek, P.; Vahtras, O.; Guo, J.; Luo, Y.; Helgaker, T.; Ågren, H. Calculations of Two-Photon Absorption Cross Sections by Means of Density-Functional Theory. *Chem. Phys. Lett.* **2003**, *374*, 446−452.
(38) Zahariev, F.; Gordon, M. S. Nonlinear Response Time-Dependent Density Functional Theory Combined with the Effective Fragment Potential Method. *J. Chem. Phys.* **2014**, *140*, 18A523.
(39) Parker, S. M.; Rappoport, D.; Furche, F. Quadratic Response Properties from TDDFT: Trials and Tribulations. *J. Chem. Theory Comput.* **2018**, *14*, 807−819.
(40) Masunov, A.; Tretiak, S. Prediction of Two-Photon Absorption Properties for Organic Chromophores Using Time-Dependent Density-Functional Theory. *J. Phys. Chem. B* **2004**, *108*, 899−907.
(41) Frediani, L.; Rinkevicius, Z.; Ågren, H. Two-Photon Absorption in Solution by Means of Time-Dependent Density-Functional Theory and the Polarizable Continuum Model. *J. Chem. Phys.* **2005**, *122*, 244104.
(42) Day, P. N.; Nguyen, K. A.; Pachter, R. Calculation of two-photon absorption spectra of donor-π-acceptor compounds in solution using quadratic response time-dependent density functional theory. *J. Chem. Phys.* **2006**, *125*, 094103.
(43) Terenziani, F.; Katan, C.; Badaeva, E.; Tretiak, S.; Blanchard-Desce, M. Enhanced Two-Photon Absorption of Organic Chromophores: Theoretical and Experimental Assessments. *Adv. Mater.* **2008**, *20*, 4641−4678.
(44) Day, P. N.; Nguyen, K. A.; Pachter, R. Calculation of One-Photon and Two-Photon Absorption Spectra of Porphyrins Using Time-Dependent Density Functional Theory. *J. Chem. Theory Comput.* **2008**, *4*, 1094−1106.
(45) Hrobáriková, V.; Hrobárik, P.; Gajdoš, P.; Fitilis, I.; Fakis, M.; Persephonis, P.; Zahradník, P. Benzothiazole-Based Fluorophores of Donor−π-Acceptor−π-Donor Type Displaying High Two-Photon Absorption. *J. Phys. Org. Chem.* **2010**, *75*, 3053−3068.
(46) Day, P. N.; Nguyen, K. A.; Pachter, R. Calculation of One- and Two-Photon Absorption Spectra of Thiolated Gold Nanoclusters using Time-Dependent Density Functional Theory. *J. Chem. Theory Comput.* **2010**, *6*, 2809−2821.
(47) Vivas, M. G.; Silva, D. L.; Misoguti, L.; Zaleśny, R.; Bartkowiak, W.; Mendonca, C. R. Degenerate Two-Photon Absorption in All-Trans Retinal: Nonlinear Spectrum and Theoretical Calculations. *J. Phys. Chem. A* **2010**, *114*, 3466−3470.
(48) De Boni, L.; Correa, D. S.; Silva, D. L.; Gonçalves, P. J.; Zilio, S. C.; Parra, G. G.; Borissevitch, I. E.; Canuto, S.; Mendonca, C. R. Experimental and Theoretical Study of Two-photon Absorption in Nitrofuran Derivatives: Promising Compounds for Photochemotherapy. *J. Chem. Phys.* **2011**, *134*, 014509.
(49) Ohta, K.; Yamada, S.; Kamada, K.; Slepkov, A. D.; Hegmann, F. A.; Tykwinski, R. R.; Shirtcliff, L. D.; Haley, M. M.; Sałek, P.; Gel'mukhanov, F.; et al. Two-Photon Absorption Properties of Two-Dimensional π-Conjugated Chromophores: Combined Experimental and Theoretical Study. *J. Phys. Chem. A* **2011**, *115*, 105−117.
(50) Palczewska, G.; Vinberg, F.; Stremplewski, P.; Bircher, M. P.; Salom, D.; Komar, K.; Zhang, J.; Cascella, M.; Wojtkowski, M.; Kefalov, V. J.; et al. Human Infrared Vision is Triggered by Two-Photon Chromophore Isomerization. *Proc. Natl. Acad. Sci. U.S.A.* **2014**, *111*, No. E5445.
(51) Di Remigio, R.; Giovannini, T.; Ambrosetti, M.; Cappelli, C.; Frediani, L. Fully Polarizable QM/Fluctuating Charge Approach to Two-Photon Absorption of Aqueous Solutions. *J. Chem. Theory Comput.* **2019**, *15*, 4056−4068.

https://doi.org/10.1021/acs.jpca.2c02395
J. Phys. Chem. A 2022, 126, 7534−7547

(52) Yu, D.; Hu, Y.; Zhang, G.; Li, W.; Jiang, Y. Theoretical studies on the two-photon absorption of II-VI semiconductor nano clusters. *Sci. Rep.* **2022**, *12*, 110.
(53) Chołuj, M.; Alam, M. M.; Beerepoot, M. T. P.; Sitkiewicz, S. P.; Matito, E.; Ruud, K.; Zaleśny, R. Choosing Bad versus Worse: Predictions of Two-Photon-Absorption Strengths Based on Popular Density Functional Approximations. *J. Chem. Theory Comput.* **2022**, *18*, 1046−1060.
(54) Nayyar, I. H.; Masunov, A. E. Two-Photon Absorption Spectra Predicted by Semiempirical Methods. *J. Comput. Theor. Nanosci.* **2014**, *11*, 2208−2220.
(55) Steindal, A. H.; Olsen, J. M. H.; Ruud, K.; Frediani, L.; Kongsted, J. A Combined Quantum Mechanics/Molecular Mechanics Study of the One- and Two-photon Absorption in the Green Fluorescent Protein. *Phys. Chem. Chem. Phys.* **2012**, *14*, 5440−5451.
(56) Salem, M. A.; Brown, A. Two-Photon Absorption in Fluorescent Protein Chromophores: TDDFT and CC2 Results. *J. Chem. Theory Comput.* **2014**, *10*, 3260−3269.
(57) Alaraby Salem, M.; Brown, A. Two-Photon Absorption of Fluorescent Protein Chromophores Incorporating Non-Canonical Amino Acids: TD-DFT Screening and Classical Dynamics. *Phys. Chem. Chem. Phys.* **2015**, *17*, 25563−25571.
(58) Salem, M. A.; Twelves, I.; Brown, A. Prediction of Two-Photon Absorption Enhancement in Red Fluorescent Protein Chromophores Made from Non-Canonical Amino Acids. *Phys. Chem. Chem. Phys.* **2016**, *18*, 24408−24416.
(59) Şimşek, Y.; Brown, A. Two-Photon Absorption Properties of Gold Fluorescent Protein: A Combined Molecular Dynamics and Quantum Chemistry Study. *J. Phys. Chem. B* **2018**, *122*, 5738−5748.
(60) Rossano-Tapia, M.; Brown, A. Determination of Two-Photon-Absorption Cross Sections Using Time-Dependent Density Functional Theory Tight Binding: Application to Fluorescent Protein Chromophores. *J. Chem. Theory Comput.* **2019**, *15*, 3153−3161.
(61) Grabarek, D.; Andruniów, T. The Role of Hydrogen Bonds and Electrostatic Interactions in Enhancing Two-Photon Absorption in Green and Yellow Fluorescent Proteins. *ChemPhysChem* **2022**, *23*, No. e202200003.
(62) List, N. H.; Olsen, J. M. H.; Jensen, H. J. A.; Steindal, A. H.; Kongsted, J. Molecular-Level Insight into the Spectral Tuning Mechanism of the DsRed Chromophore. *J. Phys. Chem. Lett.* **2012**, *3*, 3513−3521.
(63) Rossano-Tapia, M.; Brown, A. Quantum Mechanical/Molecular Mechanical Studies of Photophysical Properties of Fluorescent Proteins. *Wiley Interdiscip. Rev.: Comput. Mol. Sci.* **2022**, *12*, No. e1557.
(64) Beaujean, P.; Champagne, B.; Grimme, S.; de Wergifosse, M. All-Atom Quantum Mechanical Calculation of the Second-Harmonic Generation of Fluorescent Proteins. *J. Phys. Chem. Lett.* **2021**, *12*, 9684−9690.
(65) Grimme, S. A Simplified Tamm-Dancoff Density Functional Approach for the Electronic Excitation Spectra of Very Large Molecules. *J. Chem. Phys.* **2013**, *138*, 244104.
(66) Bannwarth, C.; Grimme, S. A Simplified Time-Dependent Density Functional Theory Approach for Electronic Ultraviolet and Circular Dichroism Spectra of Very Large Molecules. *Comput. Theor. Chem.* **2014**, *1040-1041*, 45−53.
(67) Grimme, S.; Bannwarth, C. Ultra-Fast Computation of Electronic Spectra for Large Systems by Tight-Binding Based Simplified Tamm-Dancoff Approximation (sTDA-xTB). *J. Chem. Phys.* **2016**, *145*, 054103.
(68) de Wergifosse, M.; Grimme, S. Nonlinear-response Properties in a Simplified Time-dependent Density Functional Theory (sTD-DFT) Framework: Evaluation of the First Hyperpolarizability. *J. Chem. Phys.* **2018**, *149*, 024108.
(69) de Wergifosse, M.; Grimme, S. Nonlinear-response Properties in a Simplified Time-dependent Density Functional Theory (sTD-DFT) Framework: Evaluation of Excited-State Absorption Spectra. *J. Chem. Phys.* **2019**, *150*, 094112.
(70) de Wergifosse, M.; Seibert, J.; Grimme, S. Simplified time-dependent density functional theory (sTD-DFT) for molecular optical rotation. *J. Chem. Phys.* **2020**, *153*, 084116.
(71) de Wergifosse, M.; Grimme, S. Perspective on Simplified Quantum Chemistry Methods for Excited States and Response Properties. *J. Phys. Chem. A* **2021**, *125*, 3841−3851.
(72) Katan, C.; Tretiak, S.; Werts, M. H. V.; Bain, A. J.; Marsh, R. J.; Leonczek, N.; Nicolaou, N.; Badaeva, E.; Mongin, O.; Blanchard-Desce, M. Two-Photon Transitions in Quadrupolar and Branched Chromophores: Experiment and Theory. *J. Phys. Chem. B* **2007**, *111*, 9468−9483.
(73) Homans, R. J.; Khan, R. U.; Andrews, M. B.; Kjeldsen, A. E.; Natrajan, L. S.; Marsden, S.; McKenzie, E. A.; Christie, J. M.; Jones, A. R. Two Photon Spectroscopy and Microscopy of the Fluorescent Flavoprotein, iLOV. *Phys. Chem. Chem. Phys.* **2018**, *20*, 16949−16955.
(74) Zangwill, A.; Soven, P. Density-Functional Approach to Local-Field Effects in Finite Systems: Photoabsorption in the Rare Gases. *Phys. Rev. A* **1980**, *21*, 1561−1572.
(75) Hirata, S.; Head-Gordon, M. Time-dependent density functional theory within the Tamm-Dancoff approximation. *Chem. Phys. Lett.* **1999**, *314*, 291−299.
(76) Furche, F. On the Density Matrix Based Approach to Time-Dependent Density Functional Response Theory. *J. Chem. Phys.* **2001**, *114*, 5982−5992.
(77) Wang, F.; Yam, C. Y.; Chen, G. Time-Dependent Density-Functional Theory/Localized Density Matrix Method for Dynamic Hyperpolarizability. *J. Chem. Phys.* **2007**, *126*, 244102.
(78) Thorvaldsen, A. J.; Ruud, K.; Kristensen, K.; Jørgensen, P.; Coriani, S. A density matrix-based quasienergy formulation of the Kohn-Sham density functional response theory using perturbation- and time-dependent basis sets. *J. Chem. Phys.* **2008**, *129*, 214108.
(79) Olsen, J.; Jo/rgensen, P. Linear and Nonlinear Response Functions for an Exact State and for an MCSCF State. *J. Chem. Phys.* **1985**, *82*, 3235−3264.
(80) Nishimoto, K.; Mataga, N. Electronic Structure and Spectra of Some Nitrogen Heterocycles. *Z. Phys. Chem.* **1957**, *12*, 335−338.
(81) Ohno, K. Some Remarks on the Pariser-Parr-Pople Method. *Theor. Chim. Acta* **1964**, *2*, 219−227.
(82) Klopman, G. A Semiempirical Treatment of molecular Structures. II. Molecular Terms and Application to diatomic Molecules. *J. Am. Chem. Soc.* **1964**, *86*, 4550−4557.
(83) Schmidt, M. W.; Baldridge, K. K.; Boatz, J. A.; Elbert, S. T.; Gordon, M. S.; Jensen, J. H.; Koseki, S.; Matsunaga, N.; Nguyen, K. A.; Su, S.; et al. General Atomic and Molecular Electronic Structure System. *J. Comput. Chem.* **1993**, *14*, 1347−1363.
(84) Gordon, M. S.; Schmidt, M. W.Advances in electronic structure theory. *Theory and Applications of Computational Chemistry*; Dykstra, C. E., Frenking, G., Kim, K. S., Scuseria, G. E., Eds.; Elsevier: Amsterdam, 2005; pp 1167−1189.
(85) Monson, P. R.; McClain, W. M. Polarization Dependence of the Two-Photon Absorption of Tumbling Molecules with Application to Liquid 1-Chloronaphthalene and Benzene. *J. Chem. Phys.* **1970**, *53*, 29.
(86) Wirth, M.; Koskelo, A.; Sanders, M. Molecular Symmetry and Two-Photon Spectroscopy. *Appl. Spectrosc.* **1981**, *35*, 14−21.
(87) The stda code can be obtained from: https://github.com/grimme-lab/stda/, https://github.com/grimme-lab/stda/ (accessed September 2, 2021).
(88) de Wergifosse, M.; Botek, E.; De Meulenaere, E.; Clays, K.; Champagne, B. ONIOM Investigation of the Second-Order Nonlinear Optical Responses of Fluorescent Proteins. *J. Phys. Chem. B* **2018**, *122*, 4993−5005.
(89) Pracht, P.; Bohle, F.; Grimme, S. Automated exploration of the low-energy chemical space with fast quantum chemical methods. *Phys. Chem. Chem. Phys.* **2020**, *22*, 7169−7192.
(90) Bannwarth, C.; Ehlert, S.; Grimme, S. GFN2-xTB-An Accurate and Broadly Parametrized Self-Consistent Tight-Binding Quantum Chemical Method with Multipole Electrostatics and Density-Depend-

ent Dispersion Contributions. *J. Chem. Theory Comput.* **2019**, *15*, 1652−1671.
(91) Still, W. C.; Tempczyk, A.; Hawley, R. C.; Hendrickson, T. Semianalytical Treatment of Solvation for Molecular Mechanics and Dynamics. *J. Am. Chem. Soc.* **1990**, *112*, 6127−6129.
(92) Frisch, M. J.; Trucks, G. W.; Schlegel, H. B.; Scuseria, G. E.; Robb, M. A.; Cheeseman, J. R.; Scalmani, G.; Barone, V.; Petersson, G. A.; Nakatsuji, H.; et al.*Gaussian 16*, Revision A.03; Gaussian Inc: Wallingford CT, 2016.
(93) Ehlert, S.; Bannwarth, C.; Grimme, S.Semiempirical Extended Tight-Binding Program Package xtb, version 6.2.2. https://github.com/grimme-lab/xtb/; See also xTB documentation at https://xtb-docs.readthedocs.io/en/latest/ (accessed Dec 19, 2019).
(94) Bannwarth, C.; Caldeweyher, E.; Ehlert, S.; Hansen, A.; Pracht, P.; Seibert, J.; Spicher, S.; Grimme, S. Extended Tight-Binding Quantum Chemistry Methods. *Wiley Interdiscip. Rev.: Comput. Mol. Sci.* **2020**, *11*, No. e01493.
(95) Aidas, K.; Angeli, C.; Bak, K. L.; Bakken, V.; Bast, R.; Boman, L.; Christiansen, O.; Cimiraglia, R.; Coriani, S.; Dahle, P.; et al. The Dalton Quantum Chemistry Program System. *Wiley Interdiscip. Rev.: Comput. Mol. Sci.* **2014**, *4*, 269−284.
(96) Dalton, a molecular electronic structure program. *Release Dalton2018.0*, 2018, see http://daltonprogram.org.
(97) Risthaus, T.; Hansen, A.; Grimme, S. Excited States using the Simplified Tamm-Dancoff-Approach for Range-Separated Hybrid Density Functionals: Development and Application. *Phys. Chem. Chem. Phys.* **2014**, *16*, 14408−14419.
(98) Epifanovsky, E.; Gilbert, A. T. B.; Feng, X.; Lee, J.; Mao, Y.; Mardirossian, N.; Pokhilko, P.; White, A. F.; Coons, M. P.; Dempwolff, A. L.; et al. Software for the Frontiers of Quantum Chemistry: An Overview of Developments in the Q-Chem 5 Package. *J. Chem. Phys.* **2021**, *155*, 084801.

https://doi.org/10.1021/acs.jpca.2c02395
J. Phys. Chem. A 2022, 126, 7534−7547